Annals of Anatomy 200 (2015) 98–104

Contents lists available at ScienceDirect

Annals of Anatomy

journal homepage: www.elsevier.de/aanat

Research article

Insight into the 3D-trabecular architecture of the human patella☆

Sebastian Hoechel[a,*], Georg Schulz[b], Magdalena Müller-Gerbl[a]

[a] Department of Biomedicine, Musculoskeletal Research, University of Basel, Pestalozzistrasse 20, 4056 Basel, Switzerland
[b] Biomaterials Science Center, University of Basel, Schanzenstrasse 46, 4056 Basel, Switzerland

ARTICLE INFO

Article history:
Received 13 October 2014
Received in revised form 19 January 2015
Accepted 5 February 2015

Keywords:
Human patella
Subchondral bone plate
Long-term load intake
Trabecular architecture
Micro-computed tomography

ABSTRACT

The subchondral bone plate (SBP), a dynamic component of the osteochondral unit, shows functional adaptation to long-term loading by distribution of the mineral content in a manner best serving the mechanical demands. Since the received joint-load is transmitted into the trabecular system, the spongy bone also exhibits differences in strain energy density which models it for optimal support. To evaluate the regional variations in trabecular architecture, in accordance with the density distribution of the SBP revealing its long-term load intake, CT- and μCT-datasets of ten physiologic patellae were analysed for defined parameters of bony structure. For the SBP, the density distributions as well as area measurements were used. The trabecular architecture was described using parameters of bone morphology comprising the first 5 mm (examined in 1 mm steps) below the SBP. The obtained measurements are: Bone volume fraction (BV/TV); Bone surface density (BS/TV); Trabecular number (Tb.N); Trabecular separation (Tb.Sp); Trabecular thickness (Tb.Th); structure model index (SMI); and the Degree of anisotropy (DA). The evaluated architectural parameters varied within the trabecular system and showed an inhomogeneous distribution pattern. It proved to be distinctive with maxima of material and stability situated below areas of the highest long-term load intake. With increasing depth, the pattern of distribution was persistent but lessened in intensity. The parameters significantly correlated with the density distribution of the SBP within the first and second millimetres. With increasing depth down to the fifth millimetre, the coefficients of correlation decreased for all values. The trabecular network adapts to its mechanical needs and is therefore not homogenously built. Dependent upon the long-term load intake, the trabecular model optimizes the support with significant correlation to the density distribution of the SBP.

1. Introduction

In recent years the concept of "bone's functional adaptation", often referred to as "Wolff's Law" (Wolff, 1892), has been described in literature based on the research on the osteochondral unit (OCU) of the human patella. The mechanical stimuli initiating this adaptation process are the resultant forces on the posterior patellar surface in accordance with its biomechanics.

As the largest sesamoid bone, the patella increases the functional lever arm of the quadriceps muscle by transmitting the generated forces across the knee to the tibial tubercle at a greater distance from the axis of rotation. Additionally, it centralizes the divergent forces of the quadriceps muscle and acts as a link between the quadriceps tendon and the patellar ligament. Since the tibia rotates laterally during the knee extension process, the tibial tubercle becomes laterally displaced as it is the insertion point for the patellar ligament. The remaining quadriceps angle (Q angle) between the line of application of the quadriceps force and the direction of the patellar tendon produces a lateral displacement vector of the patella on the frontal plane (Fox et al., 2012). In consequence, the lateral facet contact area is about 60% greater than the medial one which leads to a consistently greater contact force on the lateral side (Hehne, 1990; Hefzy et al., 1992; Hefzy and Yang, 1993; Fitzpatrick et al., 2011; Borotikar and Sheehan, 2013).

Following this biomechanical situation within the patellofemoral joint (PFJ), the OCU of the patella shows general signs of adaptation to the distribution of the long-term load intake. The articular as well as the subchondral bone plate (SBP) show their largest expansion on the lateral facet, with the SBP also having its maximum density and mechanical strength situated

☆ Supported by the Swiss National Science Foundation (Grant 316030_133802/1).
* Corresponding author. Tel.: +41 0 61 267 39 37.
E-mail address: sebastian.hoechel@unibas.ch (S. Hoechel).

http://dx.doi.org/10.1016/j.aanat.2015.02.007
0940-9602/

here (Eckstein et al., 1992; Milz et al., 1995; Eckstein et al., 1998; Hoechel et al., 2012).

Connected to the supporting trabecular network just below, the OCU distributes and transmits the generated strain and long-term load intake of the PFJ into this network of spongy bone and towards the anterior cortical bone of the patella.

Due to its stabilizing effect beneath the SBP, the trabecular network has increasingly become a subject of scientific interest due to its remodelling abilities. Following the idea that the trabecular architecture is arranged along the lines of the pressure it has to bear and, in this way, provides the most effective support, Humphry, as one of the first scientists to study this network, described the trabecular architecture of the proximal femur in 1858 (Humphry, 1858). Culmann and later Wolff compared these findings to an industrial crane design (Fairbairn crane) and first defined a dependency of trabecular lining to the direction of pressure generated within the human skeleton (Wolff, 1892).

For decades after, these findings on trabecular architecture were understood to be physiologic optimization to maintain integrity while minimizing bone mass. Naturally, numerous studies investigated the effects of anisotropy, connectivity as well as morphologic parameters of this network. As for the patella, the first architectural model was established in the mid-1980s by Raux and Townsend. They developed a basic model consisting of plates and interconnecting rods, which filled the space between the SBP and the dense anterior cortical bone. The most important findings document that the arrangement of trabecular differs within the patella and that zones of horizontal sheets with single axis orientation can be differentiated from zones of mixed orientation (Raux et al., 1975a,b; Townsend et al., 1976). Substantiated insights were later provided by Toumi et al., who demonstrated that the trabecular architecture varies in a complex manner between the lateral and medial facet. Their analysis of longitudinally sectioned patellae shows a significantly greater number of trabeculae orientated antero/posteriorly in the medial and central parts of the bone than laterally. Obliquely and medial–lateral orientated trabeculae were homogenously distributed in all areas of the bone. The transversely sectioned patellae revealed significantly more antero/posteriorly orientated structures in the medial and central parts, with the most obliquely aligned trabeculae were located on the lateral facet (Toumi et al., 2006a,b). Even though the analyses were performed using two-dimensional (2D) measurement techniques, the results provide remarkable insights, in having demonstrated the variation in the trabecular architecture of the patella. In addition, they reported differences in bone volume fraction between the patellar facets (Toumi et al., 2012). Unfortunately, a dependency of the internal architecture and the existing joint forces of the PFJ cannot be investigated using these methods and still remains unclear.

To investigate the theory of "form follows function" and to link the pressure distribution within the PFJ to the inside architecture of the patella, we used the established method of computed tomography osteoabsorptiometry (CT-OAM) to describe the long-term load intake of the SBP according to its density distribution. We interpreted the results in respect to the analysed 3D trabecular architecture beneath (Muller-Gerbl et al., 1989; Hoechel et al., 2012). The aim of our study is to evaluate the trabecular architecture below the SBP and describe the distinctive distribution pattern for every analysed parameter. The development of the architecture in depth will give an insight into trabecular adaptation to maintain a balanced stress level. In addition, we attempt to draw conclusions about the dependency of architectural parameters on the individual long-term load intake of the SBP.

Since the method of CT-OAM is based on conventional CT-data, the dependency of results on the CT-OAM and the trabecular architecture could be used to draw conclusions about the trabecular network in clinical routine.

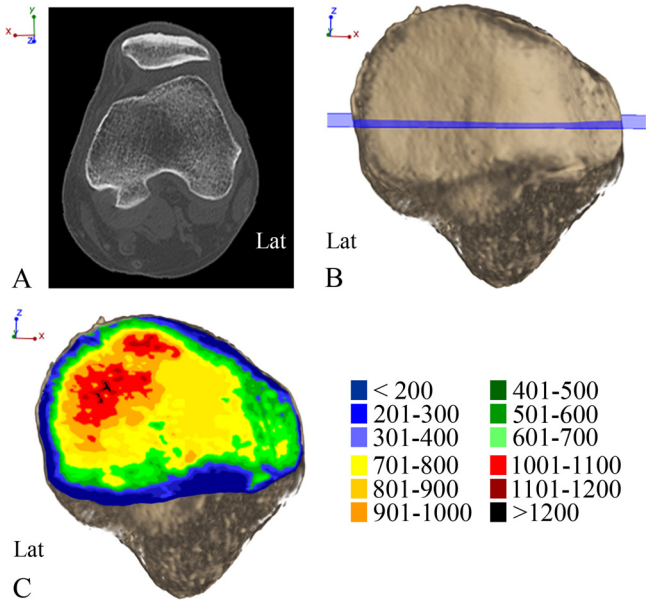

Fig. 1. Method of CT-osteoabsorptiometry of the human patella (A). Axial CT-image of a left knee (B). Isolated 3D reconstruction of the patella (posterior view), axial plane (of A) marked in blue (C). Density distribution of the subchondral bone plate of the patella including caption (in Hounsfield Units [HU]). (For interpretation of the references to color in this figure legend, the reader is referred to the web version of this article.)

2. Materials and methods

2.1. Material

A total of 10 human patellae (4% formalin concentration, fixed over 48 h, Outerbridge classification: Grade 0), acquired from donors to the Institute of Anatomy, University of Basel, Switzerland, were used. The sample population included 5 male and 5 female patellae (age 65–78, mean 72; 6 right samples, 4 left). All donors contributed their body to research at the University of Basel, Switzerland.

2.2. Methods

2.2.1. Density distribution of the SBP via CT-OAM

The CT-data required to display the density distribution in relationship to the mineralization of the SBP were generated on a conventional CT-scanner (SOMATOM 16, Siemens, Erlangen, Germany, 120 kilovolt [kV], 180 milliampere-second [mA s], slice thickness 0.6 millimetre [mm], axial slices) at the Institute of Anatomy, University of Basel, Switzerland. The CT-datasets were evaluated using the image analysing software ANALYZE® 11.0 (Biomedical Imaging Resource, Mayo Foundation, Rochester, MN, USA). After isolating the SBP of the patella, a 'maximum-intensity-projection algorithm' analysed the density distribution within. As a result, the densest voxels in posterior–anterior direction were projected onto the top of the SBP and assigned to a colour-chart where the most dense voxels (1200 Hounsfield Units [HU]) were designated black, lower values red, yellow, green and blue (in descending order, steps of 200 HU). Afterwards, the resulting image was projected onto a 3D reconstruction of the patella for anatomical orientation. The final models, representing the long-term loading history through the density distribution of the whole joint surface of the patella, served as a basis for further investigation (Fig. 1) (Muller-Gerbl et al., 1989, 1990; Muller-Gerbl, 1998; Hoechel et al., 2012).

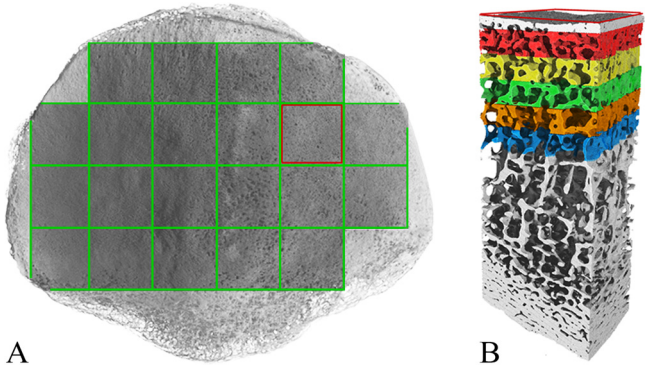

Fig. 2. Method of μ-CT; definition of measurement cube and regions of interest. (A) 3D reconstruction, left patella in dorsal view, 21 areas for extraction of measurement cubes marked. (B) Measurement cube with 5 highlighted regions of interest (1st ROI: red; 2nd ROI: yellow; 3rd ROI: green; 4th ROI: orange; 5th ROI: blue) just below the subchondral bone plate. (For interpretation of the references to color in this figure legend, the reader is referred to the web version of this article.)

2.2.2. Micro-computed tomography for evaluation of trabecular architecture

The phoenix nanotom® m is a nanoCT® system for research and industrial requirements using a 3D metrology. It creates 3D reconstructions of cross-section scans from objects up to 300 mm in diameter with voxel sizes down to 1 micrometre (μm). All samples were scanned equally using this cone-beam device with micro-focus tube, acceleration voltage 140 kV, at a beam current of 60 mA s. In addition, a 0.5 mm aluminium filter was used to minimize beam hardening. Each scan included 2100 projections from 360 degrees. The resulting isotropic voxel size of the generated images accounted for 32 μm. The nanotom® m reconstruction of the 3D dataset is based on a modified Feldkamp algorithm which integrated the patella fractions into one 3D object (Feldkamp et al., 1984).

With the help of VGStudio® Max 2.2 (Heidelberg, Germany), each 3D dataset was virtually divided into 21 measurement cubes. Cube measurements: proximal-distal: 8 mm, lateral–medial: 8 mm, posterior–anterior: SBP to the anterior cortical bone. The remaining odd measurement cubes were neglected since here the SBP is not supported by trabeculae of any kind as it is in direct contact with the anterior cortical bone (Fig. 2).

On every measurement cube, the first five mms of trabecular bone just beneath the SBP were divided into five, equally sized ($8 \times 8 \times 1$ mm) regions of interest (ROI). 1st ROI: 0–1 mm of trabecular bone just below the SBP, 2nd ROI: 1–2 mm of trabecular bone below the SBP, likewise for the 3rd, 4th, and 5th ROI (Fig. 2B). Measurements of trabecular architecture were performed equally on all ROIs for all cubes with the help of the Skyscan software CT-analyser® (Bruker-Microct, Belgium).

2.2.3. Obtained parameters for analysis

In accordance with the literature and the described main parameters of trabecular bone architecture:

(a) BV/TV (%), Bone volume fraction
(b) BS/TV (1/mm), Bone surface density
(c) Tb.Th (mm), Trabecular thickness
(d) Tb.Sp (mm), Trabecular separationas primary measurements in bone histomorphometry (Hildebrand et al., 1999).

Derived indices:

(e) Tb.N (1/mm), Trabecular numberas structural parameter (Parfitt et al., 1987; Hildebrand et al., 1999). As well as:
(f) SMI (dimensionless), Structure model index
(g) DA (dimensionless), Degree of anisotropyto directly quantify the otherwise subjective classification of plate-like and rod-like trabecular architecture and to assess the 3D symmetry of it (Hildebrand and Ruegsegger, 1997).

For evaluation, the data of the ROIs of the measurement cubes was assigned to five layers and represented in 2D distribution charts. Therefore, every assessed parameter of the 1st ROIs was reassembled in one layer, stating the distribution of this parameter across the articular network of the patella. Likewise the data was arranged down to the 5th ROIs of all measurement cubes (fifth layer) (Fig. 3).

In addition to these trabecular data, the mean density (HU) of the SBP of every measurement cube was derived from the density distribution charts compiled via CT-OAM. The results were tabulated and assigned to the corresponding trabecular dataset.

2.2.4. Statistics

For all appraised samples, the Pearson product-moment correlation coefficient was established. Using a two-tailed *t*-test, the significance was performed. For analysis of data distribution, the Kolmogorov–Smirnov test was used. All statistical analyses were done using RStudio (RStudio: Integrated-development environment for R, Version 0.96.122, Boston, MA, USA).

3. Results

3.1. Density distribution of the SBP via CT-OAM

The results showed the peak density area to be consistently located on the lateral facet. Originating at this localization of highest density, a steady decrease was found towards the periphery. Density values recorded on the medial facet have a considerably lower absolute value (Fig. 1, representative sample). The maxima on the lateral side, however, showed substantial inter-individual differences. The peak values of the maxima varied from 928 HU to 1411 HU, lowest density values of all samples ranged from 282 HU to 658 HU.

3.2. Parameters of trabecular bone

(a) BV/TV, (b) BS/TV; within the 2D distribution charts, the distribution of bone and bone surface density is inhomogeneous in every analysed layer (Fig. 3). Consistently, maxima of bone volume and surface density are found beneath the lateral facet, decreasing into the periphery. The medial facet shows significantly ($p > 0.05$) lower values. The pattern of distribution reveals a consistency into depth, where the parameters show a peak on the lateral facet as well. The range of maximum and minimum values gradually decreases with depth as the distribution becomes more homogenous.

The decrease of bone volume and bone surface density with every layer of depth is visualized in Fig. 4.

(c) Tb.Th, (e) Tb.N; again, the maxima of these parameters are found below the lateral facet, with values decreasing into the periphery. The pattern also showed consistency down to the 5th mm (Figs. 3 and 4).

(d) Tb.Sp; the trabecular separation differs across the trabecular architecture as well but proved to have a persistent minimum below the lateral facet, representing packed stacks of trabecular bone. The highest values, interpreted as loose formation of trabecular are found below the medial facet and in the periphery (Fig. 3). Overall, highest and lowest values found within the 1st layer increasing with depth (Fig. 4).

(f) SMI; within the analysed sample population, we found plate-like trabecular mainly below the lateral facet. Rod-like architecture was seen below the medial part and in the periphery. The pattern of

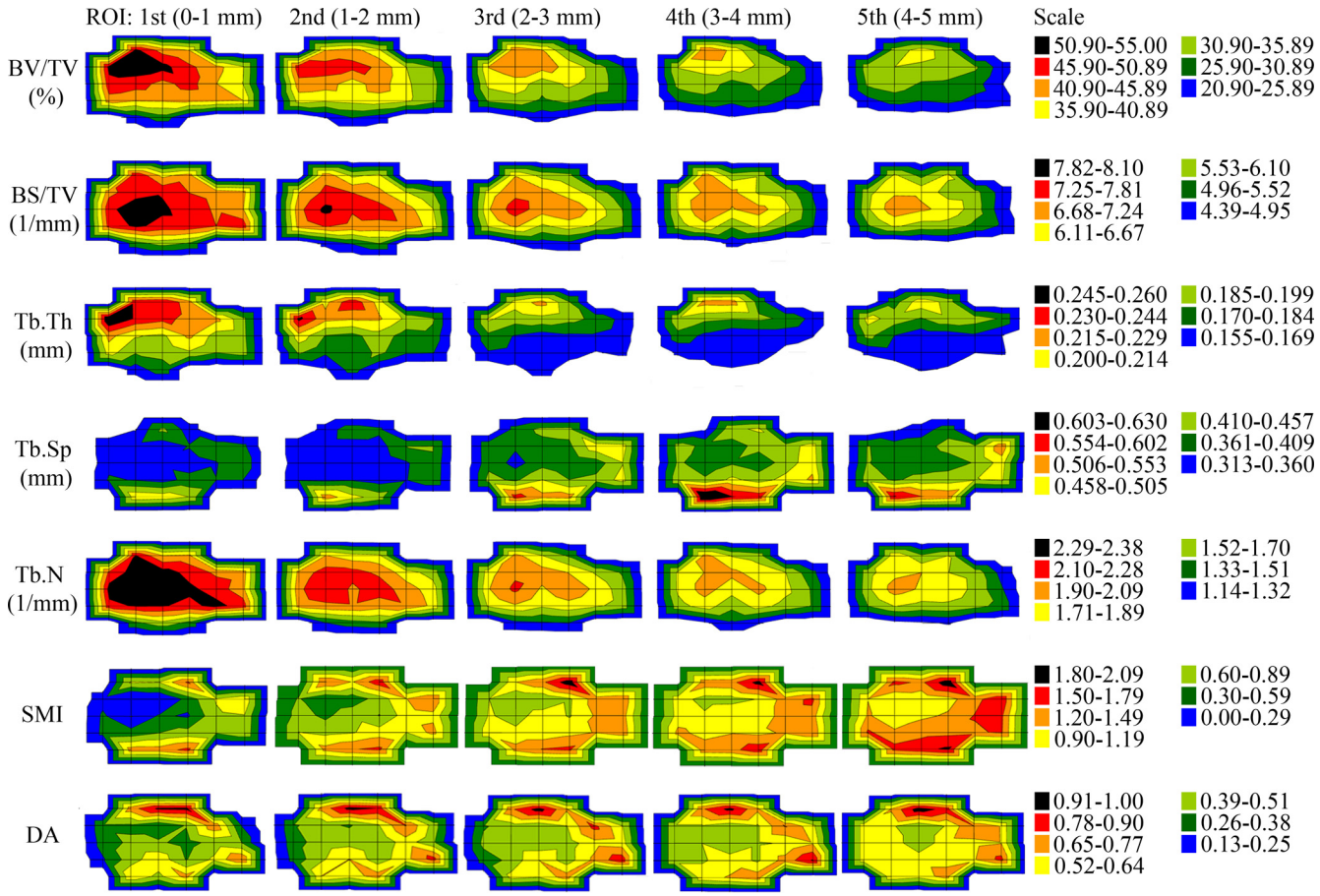

Fig. 3. 2D distribution charts of trabecular architectural parameters for the five analysed ROIs from the first to the fifth millimetre (same sample and orientation as Fig. 2).

Table 1
Mathematical description of the dependency of trabecular parameters of the human patella and the according depth (1st to the 5th ROI) as presented in Fig. 4.

Parameter	Dependency of (x) and (y)	Correlation*
BV/TV	$y = -8.76\ln(x) + 37.05$	$r^2 = 0.99$
BS/TV	$y = -1.03\ln(x) + 6.65$	$r^2 = 1.00$
Tb.Th	$y = -0.02\ln(x) + 0.19$	$r^2 = 0.98$
Tb.Sp	$y = 0.07\ln(x) + 0.36$	$r^2 = 1.00$
Tb.N	$y = -0.34\ln(x) + 1.91$	$r^2 = 1.00$
SMI	$y = 0.35\ln(x) + 0.76$	$r^2 = 1.00$
DA	$y = 0.03\ln(x) + 0.53$	$r^2 = 0.98$

(x) = depth below the subchondral bone plate (mm), (y) = parameter value.
* Correlation of logarithmic dependency to measured mean values (Fig. 4).

distribution continued down to the 5th layer (Fig. 3), the absolute values of the SMI increased (Fig. 4).

(g) DA; we found an area of isotropic constellation below the lateral facet within the 1st layer of ROIs, which changed into a more anisotropic state with depth. The medial part as well as areas in the periphery showed higher values expressing a more anisotropic state that increased with depth. The distribution pattern persisted down to the 5th layer with the differences between maximum and minimum reducing gradually (Fig. 3). The overall anisotropy increased with depth (Fig. 4).

The overall change in absolute values of every parameter (Fig. 4, y-axes) that occurs with depth (Fig. 4, x-axes) shows a logarithmic dependency (Table 1).

3.3. Trabecular bone parameters in correlation with density distribution of the SBP

Positive correlation coefficients were found for BV/TV, BS/TV, Tb.Th, and Tb.N. These parameters showed the highest correlation within the 1st analysed layer (r^2 up to 0.81). Down to the 5th layer, there was a steady decrease to $r^2 = 0.25$ (Table 2).

The Tb.Sp, SMI, and DA described a high negative correlation. Values of up to $r^2 = -0.82$ for the 1st layer also steadily decreased with depth down to values as low as $r^2 = -0.29$ in the deepest evaluated layer (Table 2).

4. Discussion

The idea of bony tissue not being rigid and inflexible is not new in literature. First publications describing the phenomenon of bone adaptation to imposed mechanical loadings can be found as early as in the 19th century, when shortly after, the femoral head was described as “highly motivated” by Karl Culmann and the ideas at that time were summarised and substantiated by Wolff (1892) and Bourgery (1854). The cornerstone of his work is the interpretation of the internal alignment of the trabeculae. Following along the principal stress directions expected from functional load bearing, the pattern of the trabecular framework is described as ‘controlled’ by the direction of the load acting onto the bone. Wolff further proposed that the orientation of trabeculae is transformable with alterations in loading pattern. His hypothesis and rules of transfiguration are still known as “Wolff’s Law” today (Wolff, 1892). Since then, the methods of macroscopic analysis and the in vitro assessment of bony structures developed towards a microscopic level. Thin section analysis, acquired either by sawing or cutting, is currently the most established method to describe and quantify structural parameters of trabecular bone. The disadvantages of these long-established methods are the interpretation of 2D sections and the use of mathematical models for extrapolation to

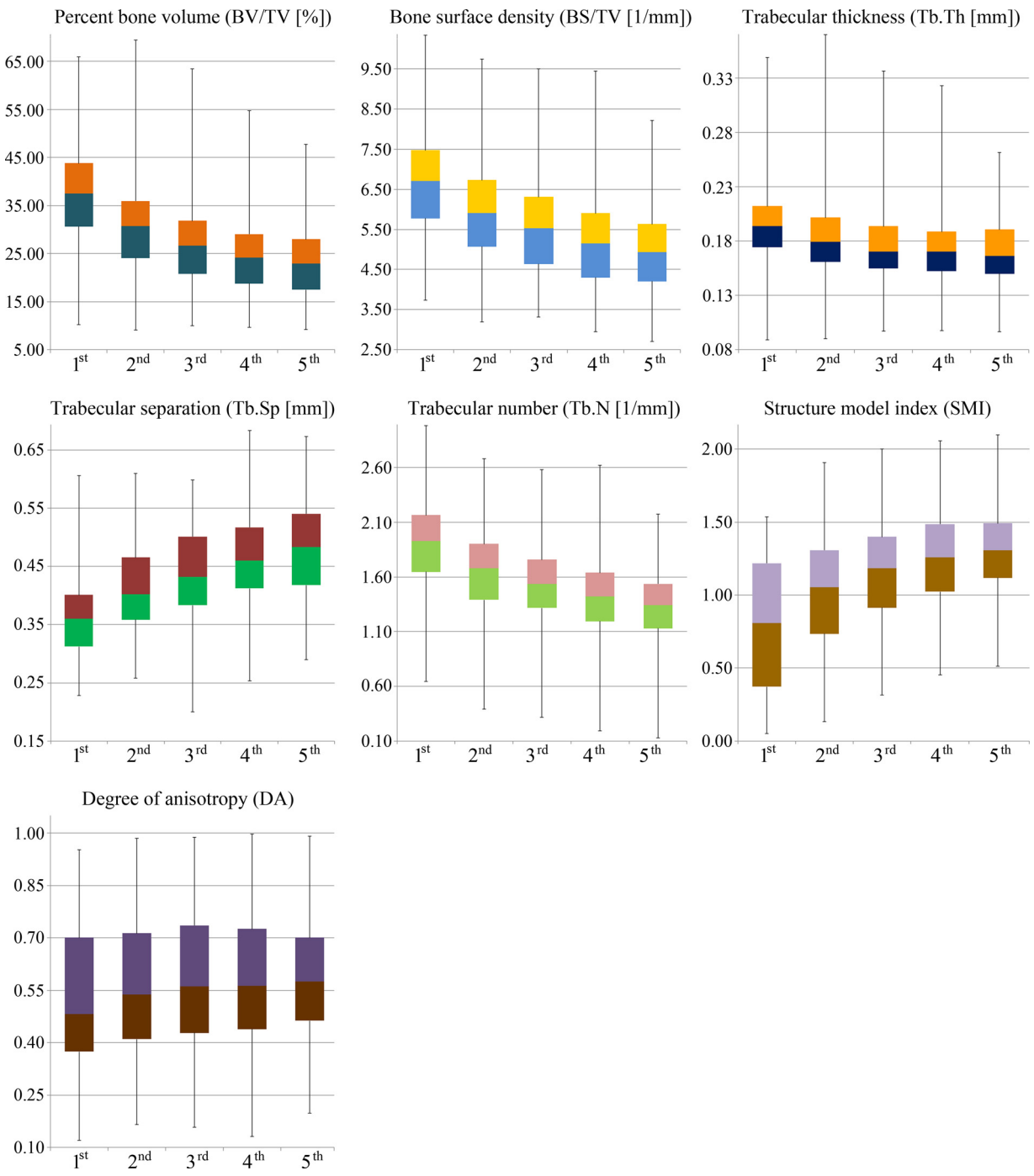

Fig. 4. Box-and-whisker plot of the development of the architectural parameter values of the trabecular network from the 1st to the 5th ROI below the subchondral bone plate of all samples (whiskers representing one standard deviation above and below the mean of the data).

Table 2
Trabecular bone parameters in correlation to density distribution of the SBP.

mm	BV/TV	BS/TV	Tb.Th	Tb.Sp	Tb.N	SMI	DA
0–1	0.81 (0.06)	0.81 (0.06)	0.73 (0.08)	−0.70 (0.10)	0.76 (0.13)	−0.82 (0.10)	−0.71 (0.05)
1–2	0.74 (0.09)	0.74 (0.11)	0.55 (0.14)	−0.55 (0.19)	0.63 (0.29)	−0.68 (0.26)	−0.65 (0.12)
2–3	0.62 (0.14)	0.62 (0.18)	0.44 (0.14)	−0.49 (0.26)	0.59 (0.27)	−0.56 (0.24)	−0.56 (0.12)
3–4	0.49 (0.19)	0.49 (0.23)	0.32 (0.22)	−0.54 (0.16)	0.58 (0.21)	−0.50 (0.29)	−0.46 (0.14)
4–5	0.44 (0.18)	0.44 (0.22)	0.25 (0.21)	−0.24 (0.33)	0.48 (0.22)	−0.39 (0.33)	−0.29 (0.18)

(. . .) = standard deviation.

the 3D arrangement which consistently lead to false assumptions (Engelke et al., 1999).

Today, microcomputer tomography presents an emerging alternative to histomorphometry. Time-consuming preparation like cutting, staining, or radiologic analysis of serial sections is redundant and the analysis is of direct character without interpolation based on mathematical models and the assumption of the 3D architecture. Since the initial technical limitations improved greatly, it is possible to evaluate complete bones and describe the architecture of the whole 3D trabecular network at once. As for the patella, we were able to map the architecture of the trabecular network below the whole articular surface and directly represent it.

The biomechanics of the PFJ are mainly influenced by the setting of the extensor mechanism using the patella as a pulley. Being the focus for the insertions of the large quadriceps muscle at its top, the patella also serves as an insertion point for the patellar ligament at its base. Together, the applied forces acting on the small mobile bone with an incongruent geometry lead to large contact stress (Amis and Farahmand, 1996). As the knee flexes and the patella slides into the trochlear groove, the patellofemoral contact initiates at the distant pole and moves upwards with increasing flexion (Aglietti et al., 1975). Due to the valgus angulation between the resultant line of action of the quadriceps muscle and the patellar tendon, the resultant force is directed against the lateral margin of the femoral trochlea (Hehne, 1990). This way, the greater area of contact is located on the lateral facet of the patella where the peak strain is also situated (Goodfellow et al., 1976; Scuderi, 1995; Fitzpatrick et al., 2011). With increasing extension, the peak strain on the patella moves in a distal and medial direction, always staying on the lateral facet (Borotikar and Sheehan, 2013). Adapting to this pressure transmission, the articular cartilage and the SBP beneath are known to show the maximum thickness, density, and strength here (Eckstein et al., 1992; Hoechel et al., 2012). The SBPs density distribution of the human patella can therefore be regarded as representing the long-term loading history (Muller-Gerbl et al., 1989; Muller-Gerbl, 1998).

The analysis of the trabecular architecture just below the SBP revealed structural properties in accordance with the biomechanical situation represented. It was not at all surprising that the parameters of BV/TV, BS/TV, Tb.Th, and Tb.N showed maxima just beneath the regions of maximal density in the SBP, which describe an accumulation of bone in order to maximize the support here. The reported maxima decreased into the periphery and showed less trabecular bone in the region of the patellar ridge and the medial facet just like the density distribution. Interestingly, these distribution patterns of trabecular bone are found to be consistent in the analysed depth of the trabecular system. Showing significant lower overall levels in the deeper layers, the distribution with maxima beneath the densest area is found down to the fifth millimetre. Next to this quantitative support, the parameters resembling the structure revealed the most stable arrangement beneath zones of highest load intake. The SMI described primarily a plate formation here, which changed into rods in the periphery. The DA of these trabecular indicates the most interconnections in between the plates whereas the periphery with less long-term load intake is designed with unconnected rods. The arrangement of the trabecular therefore shows not only the most material but also the strongest arrangement just beneath areas of highest load intake. Its arrangement is a direct result of mechanical input forming a distinctive architectural pattern in order to support the SBP in an optimal compromise of structure and material use.

Following high correlations of trabecular architectural parameters to the density distribution of the SBP within the first and second mm of analysed trabecular bone, the resulting force seems afterwards to be spread within the trabecular system in such a way that the inhomogeneous structure distribution with high differences of absolute values gradually becomes more homogenous, the differences in absolute level decrease and the correlation to the distinctive long-term load intake of the SBP lessens.

The described structural properties can be interpreted following the "Mechanobiology hypothesis" of Carter and Beaupré (Carter, 1984; Carter et al., 2007). Next to the biological component (r_b) of the genetic disposition of bone which is dominant during the juvenile growth period, the mechanical (r_m) component models bone in a way to experience optimum strain levels. This described strain energy density (SED) within the trabecular network is the summation of single load intake moments which is defined as "loading history" over a period of time where the differences in SED distribution over the articular surface seem to administer the delicate differentiation of each structural parameter. The trabecular adaptation changes from a high degree of differentiation just beneath the SBP to a more equal distribution within the lower analysed layers. This in the end creates a state of homeostasis between structural arrangement and equally distributed SED. But it is more than probable, that bone cells respond more to components of their mechanical environment than just physical deformation by the generated strain.

On a cellular level, the in vivo loading always triggers a fluid flow within the widely spaced lacunae interconnected by canaliculi. The produced oscillatory fluid flow results in a cell response via streaming potentials, chemo-transport and wall shear stress. The latter is believed to stimulate cell wall processes causing cell deformation and subsequent metabolic activity (Jacobs et al., 1998; Lanyon and Skerry, 2001; Wang et al., 2004).

The resulting trabecular architecture stimulated by these processes is therefore in strong correlation to the load and strain distribution of the articular surface. The forces transmitted from above form the network towards a distinct, optimally supportive architectural pattern as shown in this work. The spreading and absorption of these forces on their way into the depth of the trabecular network leads to an equalization of this network, once the distribution is homogeneous. This development can be mathematically accessed for every single parameter. The calculations and results presented are specifically for the patella and for a physiological condition only.

The data in this work concretises the previously described architectural arrangement of different plate orientations and differences in quantity of bony material across the trabecular network observed from 2D slices (Raux et al., 1975a,b; Townsend et al., 1975, 1976). Differences to the data observed by above mentioned authors as well as by Toumi et al. (2006a,b) result in the areas observed. In contrast to their research including the anterior trabeculae close to the cortical bone, we intentionally focussing on the trabeculae within the first 5 mm below the SBP with direct pressure intake through the joint.

With the help of μCT analysis of these trabeculae which receive the unaltered joint-pressure distribution via the SBP, the directly approached link of the biomechanics of the single patella through analysis of the long-term load intake in union with the trabecular structure can be approached. It reveals the highly differentiated architecture as a result of adaptation to optimize the support and strain distribution. The adaptations, generated by osteocytes in dependency on their local load and strain intake, can altogether advance the understanding of the form-function relation.

Even though the data describes the coherence of the above-mentioned structures, information about bone remodelling on a cellular level cannot be provided using μCT. In order to interpret the presented data for the forming and reabsorption of trabecular bone, histochemical and immunohistochemical demonstration of alkaline phosphatase activity of the subchondral bone will be performed. Since it has been suggested that subchondral

bone remodelling plays an important role in the progression of osteoarthritis where the exact pathogenesis still remains unclear, we will include osteoarthritic samples in the upcoming studies to compare to this data (Van den Berg, 2011).

Acknowledgements

Sebastian Hoechel and Magdalena Müller-Gerbl designed the study. Georg Schulz developed the technical implementation and supervised the use of the phoenix nanotom® m. Sebastian Hoechel collected the data, developed the methodology, and wrote the manuscript.

We kindly thank the Swiss National Science Foundation for their financial support with the acquisition of the phoenix nanotom® m (R'Equip program, Grant 316030_133802/1).

Furthermore, we would like to thank Mrs. Christine Müller-Thompson for the support with editing and typesetting of this manuscript.

Appendix A. Supplementary data

Supplementary data associated with this article can be found, in the online version, at http://dx.doi.org/10.1016/j.aanat.2015.02.007.

References

Aglietti, P., Insall, J.N., et al., 1975. A new patella prosthesis: design and application. Clin. Orthop. Relat. Res. 107, 175–187.
Amis, A., Farahmand, F., 1996. Extensor mechanism of the knee. Curr. Orthop. 10 (2), 102–109.
Borotikar, B., Sheehan, F., 2013. *In vivo* patellofemoral contact mechanics during active extension using a novel dynamic MRI-based methodology. Osteoarthritis Cartilage 21 (12), 1886–1894.
Bourgery, J.-B.-M., 1854. Traité complet de l'anatomie de l'homme comprenant la médecine opératoire.
Carter, D.R., 1984. Mechanical loading histories and cortical bone remodeling. Calcif. Tissue Int. 36 (1), S19–S24.
Carter, D.R., Beaupré, G.S., et al., 2007. Skeletal Function and form: Mechanobiology of Skeletal Development, Aging, and Regeneration. Cambridge University Press, Cambridge.
Eckstein, F., Milz, S., et al., 1998. Thickness of the subchondral mineralised tissue zone (SMZ) in normal male and female and pathological human patellae. J. Anat. 192 (Pt 1), 81–90.
Eckstein, F., Muller-Gerbl, M., et al., 1992. Distribution of subchondral bone density and cartilage thickness in the human patella. J. Anat. 180 (Pt 3), 425–433.
Engelke, K., Karolczak, M., et al., 1999. Micro-CT. Technology and application for assessing bone structure. Der Radiologe 39 (3), 203–212.
Feldkamp, L., Davis, L., et al., 1984. Practical cone-beam algorithm. JOSA A 1 (6), 612–619.
Fitzpatrick, C.K., Baldwin, M.A., et al., 2011. Comparison of patellar bone strain in the natural and implanted knee during simulated deep flexion. J. Orthop. Res. 29 (2), 232–239.
Fox, A.J., Wanivenhaus, F., et al., 2012. The basic science of the patella: structure, composition, and function. J. Knee Surg. 25 (02), 127–142.
Goodfellow, J., Hungerford, D., et al., 1976. Patello-femoral joint mechanics and pathology. 1. Functional anatomy of the patello-femoral joint. J. Bone Joint Surg. (British Volume) 58 (3), 287–290.
Hefzy, M., Jackson, W., et al., 1992. Effects of tibial rotations on patellar tracking and patello-femoral contact areas. J. Biomed. Eng. 14 (4), 329–343.
Hefzy, M., Yang, H., 1993. A three-dimensional anatomical model of the human patello-femoral joint, for the determination of patello-femoral motions and contact characteristics. J. Biomed. Eng. 15 (4), 289–302.
Hehne, H.-J., 1990. Biomechanics of the patellofemoral joint and its clinical relevance. Clin. Orthop. Relat. Res. 258, 73–85.
Hildebrand, T., Laib, A., et al., 1999. Direct three-dimensional morphometric analysis of human cancellous bone: microstructural data from spine, femur, iliac crest, and calcaneus. J. Bone Miner. Res. 14 (7), 1167–1174 (The Official Journal of the American Society for Bone and Mineral Research).
Hildebrand, T., Ruegsegger, P., 1997. Quantification of bone microarchitecture with the structure model index. Comput. Methods Biomech. Biomed. Eng. 1 (1), 15–23.
Hoechel, S., Wirz, D., et al., 2012. Density and strength distribution in the human subchondral bone plate of the patella. Int. Orthop. 36 (9), 1827–1834.
Humphry, G.M., 1858. A Treatise on the Human Skeleton. Macmillan, New York.
Jacobs, C., Yellowley, C., et al., 1998. Differential effect of steady versus oscillating flow on bone cells. J. Biomech. 31 (11), 969–976.
Lanyon, L., Skerry, T., 2001. Perspective: postmenopausal osteoporosis as a failure of bone's adaptation to functional loading: a hypothesis. J. Bone Miner. Res. 16 (11), 1937–1947.
Milz, S., Eckstein, F., et al., 1995. The thickness of the subchondral plate and its correlation with the thickness of the uncalcified articular cartilage in the human patella. Anat. Embryol. (Berl.) 192 (5), 437–444.
Muller-Gerbl, M., 1998. The subchondral bone plate. Adv. Anat. Embryol. Cell Biol. 141 (III–XI), 1–134.
Muller-Gerbl, M., Putz, R., et al., 1989. Computed tomography-osteoabsorptiometry for assessing the density distribution of subchondral bone as a measure of long-term mechanical adaptation in individual joints. Skeletal Radiol. 18 (7), 507–512.
Muller-Gerbl, M., Putz, R., et al., 1990. Demonstration of subchondral density pattern using CT-osteoabsorptiometry (CT-OAM) for the assessment of individual joint stress in live patients. Zeitschrift fur Orthopadie und ihre Grenzgebiete 128 (2), 128–133.
Parfitt, A.M., Drezner, M.K., et al., 1987. Bone histomorphometry: standardization of nomenclature, symbols, and units: report of the ASBMR Histomorphometry Nomenclature Committee. J. Bone Miner. Res. 2 (6), 595–610.
Raux, P., Townsend, P.R., et al., 1975a. Trabecular architecture of the human patella. J. Biomech. 8 (1), 1–7.
Raux, P., Townsend, P.R., et al., 1975b. Trabecular architecture of the human patella. J. Biomech. 8 (1), 1–7.
Scuderi, G.R., 1995. The patella. Springer, New York.
Toumi, H., Higashiyama, I., et al., 2006a. Regional variations in human patellar trabecular architecture and the structure of the proximal patellar tendon enthesis. J. Anat. 208 (1), 47–57.
Toumi, H., Higashiyama, I., et al., 2006b. Regional variations in human patellar trabecular architecture and the structure of the proximal patellar tendon enthesis. J. Anat. 208 (1), 47–57.
Toumi, H., Larguech, G., et al., 2012. Regional variations in human patellar trabecular architecture and the structure of the quadriceps enthesis: a cadaveric study. J. Anat. 220 (6), 632–637.
Townsend, P.R., Miegel, R.E., et al., 1976. Structure and function of the human patella: the role of cancellous bone. J. Biomed. Mater. Res. 10 (4), 605–611.
Townsend, P.R., Raux, P., et al., 1975. The distribution and anisotropy of the stiffness of cancellous bone in the human patella. J. Biomech. 8 (6), 363–367.
Van den Berg, W., 2011. Osteoarthritis year 2010 in review: pathomechanisms. Osteoarthritis Cartilage 19 (4), 338–341.
Wang, L., Ciani, C., et al., 2004. Delineating bone's interstitial fluid pathway in vivo. Bone 34 (3), 499–509.
Wolff, J., 1892. Das Gesetz der Transformation der Knochen. Hirschwald, Berlin.